Applied Catalysis A: General 477 (2014) 26–33

Contents lists available at ScienceDirect

Applied Catalysis A: General

journal homepage: www.elsevier.com/locate/apcata

A new peroxo-route for the synthesis of Mg–Zr mixed oxides catalysts: Application in the gas phase acetone self-condensation

Igor Krivtsov[a], Laura Faba[b], Eva Díaz[b], Salvador Ordóñez[b,*], Viacheslav Avdin[a], Sergei Khainakov[c], Jose R. Garcia[c]

[a] Nanotechnology Research and Education Center, Department of Chemistry, South Ural State University, Lenina av. 76, Chelyabinsk, Russia
[b] Department of Chemical and Environmental Engineering, University of Oviedo, JuliánClavería s/n, Oviedo 33006, Spain
[c] Department of Organic and Inorganic Chemistry, University of Oviedo, JuliánClavería s/n, Oviedo 33006, Spain

ARTICLE INFO

Article history:
Received 20 December 2013
Received in revised form 3 March 2014
Accepted 4 March 2014
Available online 13 March 2014

Keywords:
Magnesia–zirconia
Acetone condensation
Aldol condensation
Zirconium peroxocomplex

ABSTRACT

We propose in this manuscript a new peroxo-mediated procedure for preparing magnesia–zirconia mixed oxides, with Mg/Zr molar ratio between 1 and 3, with enhanced distribution of basic sites. The mixed magnesia–zirconia oxides have been prepared from the gelled complex by Pechini-type method. The $MgO–ZrO_2$ materials have been characterized and used as catalysts for acetone aldol condensation. The proposed preparation method provides a high degree of molecular homogeneity and favours the formation of magnesia-stabilized zirconia phase. Acetone gas-phase self-condensation was carried out over these catalysts as model reaction requiring the presence of basic sites. The condensation yields diacetone alcohol and mesityl oxide as mean C6 products, and phorones, isophorones and mesitylene as C9 products. In comparison to Mg–Zr oxide prepared by co-precipitation, these new materials present better conversions and higher selectivity to linear dimers and trimers (as mesitylene), whereas the selectivity for isophorones is significantly lower.

1. Introduction

Complex oxides of IV group of elements of the periodic table and alkaline earth metals have attracted great attention of scientists and industry for a long time, since they can be used as conductive ceramics [1], biocompatible materials [2], adsorbents [3], and catalysts [4]. This last application is growing up in importance due to the arising demand of catalysts with both basic and acid sites [5–10]. In the case of magnesia–zirconia catalysts, the most common preparation procedure is the co-precipitation of the inorganic salts, nitrates or chlorides [11], and more rarely ultra-dilution methods [12], and citrate- or oxalate processing [13,14]. The processes of phase formation, polymorphic transitions (in precipitated magnesia–zirconia or prepared via conventional sol–gel Pechini-method) as well as their surface properties, are thoroughly studied [15,16]. However, it is known that many properties of sol–gel or precipitated materials based on zirconia are determined by factors such as the salt anion used in the synthesis [17], the pH of the reaction mixture and even the order of mixing with precipitating agent [18]. These parameters affect the properties and the structure of the final product as they determine the hydrolysis rate, and the oligomerization and polymerization of aqueous complexes of zirconium, not existing in monomeric form even in very acidic medium. Application of alkoxides solves some problems by controlling the hydrolysis and polymerization of zirconia species and, as result, high surface area mesoporous materials are obtained [19]. Alkoxide sol–gel technique has proved to be the best method to prepare high performance metal oxide catalysts, but it has several disadvantages standing on the way of its application on industrial scale. Alkoxides are much more expensive than inorganic salts, unstable and easily hydrolyzed under the influence of atmospheric water vapors, thus special precautions are necessary when handling them [20]. Furthermore, alkoxides are highly toxic compounds and a great amount of organic solvents is indispensable during alkoxide-based sol–gel synthesis, thus, they do not meet requirements of sustainable chemical processes.

The peroxocomplexes of some transition metals could be considered as a “green” alternative to metal alkoxide precursors [21]. Although, different studies on the synthesis of peroxocomplexes [21,22] have been reported, studies on zirconium peroxocomplexes as the precursors for ZrO_2 or zirconium-based complex oxides are scarce. Gao et al. [23] reported the peroxo-method for zirconia

* Corresponding author. Tel.: +34985103437; fax: +34985103434.
E-mail address: sordonez@uniovi.es (S. Ordóñez).

http://dx.doi.org/10.1016/j.apcata.2014.03.008
0926-860X/

thin-film preparation, whereas Park et al. [24] found some advantages of peroxo-mediated procedure for ZrO_2 films synthesis, as such as the homogeneous distribution on the substrate and high density of the film. High degree of homogeneity of the complex oxide is also found to be one of the advantages of peroxo-routes, as it allows lowering the temperatures of heat treatment while obtaining the desirable phase [25,26].

A deep knowledge about the characteristics of mixed oxides of magnesia and zirconia is of key importance in basic heterogeneous catalysis. Mixed MgO/ZrO_2 has shown high catalytic activity in furfural aldol condensation with acetone [27] and, as it has recently been reported, in gaseous acetone self-condensation [28]. Acetone self-condensation is a highly important industrial and scientifically interesting reaction, since emerging chemical and biological processes have become the acetone into a bio-based platform molecule. Upgrading of acetone relies on the formation of new C–C bonds, yielding more complex molecules, being mesityl oxide, isophorones, and mesitylene the most interesting products [29]. Despite the great interest of this reaction, the reasons for selectivity towards certain products are still unclear to the researchers, since many properties of the catalysts have influence on the way of the reaction. It is likely that not only the distribution of acid-basic sites determines the activity and selectivity of the catalyst, but also the degree of molecular mixing in the oxide may play a significant role, as it has been pointed out by Sádaba et al. [30].

A new procedure for the preparation of MgO/ZrO_2 mixed oxides (using water-soluble peroxocomplex as precursors) is reported, describing their structural, textural and physicochemical properties, and correlating these properties with the catalytic performance in the gas phase acetone self-condensation.

2. Experimental

2.1. Chemicals

Mixed magnesia–zirconia oxides were prepared using magnesium sulfate ($MgSO_4$) obtained from Prolabo (98% pure) and zirconium oxychloride aqueous solution ($ZrOCl_2$), containing 19–21 wt% of ZrO_2, purchased from MEL Chemicals as MgO and ZrO_2 sources, respectively. Hydrogen peroxide 30 wt% water solution, anhydrous citric acid (97% pure) and acetone (99.8% pure) were supplied by Aldrich; whereas sodium hydroxide (99%pure) was supplied by Prolabo. All chemicals were used as received without further purification. As zirconium salts usually form polymeric hydroxo-species in aqueous solution, leading to precipitation and changing of concentration, the content of zirconium was determined gravimetrically prior to its use for synthesis.

2.2. Synthesis of MgO/ZrO_2 mixed oxides

A new peroxocomplex-mediated route to prepare mixed magnesia–zirconia oxides was accomplished in several stages. Several steps are coincident with a procedure described earlier for the preparation of SiO_2/TiO_2 mixed oxides [31]. In the first stage, the conventional co-precipitation procedure described by Aramendia et al. [11] was applied. Initially, the starting aqueous solutions of $MgSO_4$ (0.2, 0.4 and 0.6 M concentrations were used in order to achieve the desired Mg/Zr ratio) and 50-mL of $ZrOCl_2$ (0.2 M) were mixed and precipitated while stirring with 1.5 M NaOH solution at pH value equal to 10.7. The rate of stirring of a magnetic stirrer varied from 200 rpm in the beginning of the precipitation to 600 rpm when the suspension became viscous. The prepared precipitates were centrifuged at 3000 rpm and washed 8 times with deionized water to remove sodium sulfates and chlorides. The peroxocomplexes were prepared in the following way: the mixture formed by 20 mL of H_2O_2 and 20 mmol of anhydrous citric acid was added to the precipitates, the obtained suspensions were heated at 373 K under stirring (200 rpm) for 15 min. The precipitate with Mg/Zr = 3 was totally dissolved and clear solution was obtained, whereas in other cases the precipitates dissolution was incomplete and the solution was isolated from the solid phase by centrifugation at 3000 rpm. The final stage of the synthesis was accomplished via Pechini-type sol–gel process. Water from the solutions was evaporated on a water bath that caused gelation, then gels were dried in an oven at 333 K for 24 h, powdered in an agate mortar, heated at 473 K for 3 h (for decomposition of the complexes), and finally treated at 873 K for 4 h in air to obtain mixed oxides with Mg/Zr molar ratios equaling 1.0, 2.0 and 3.0 (further designated as 1MZ, 2MZ and 3MZ). Solid water-soluble peroxocomplexes were also subjected to investigation. First, they were isolated from water solutions by precipitation with ethanol. The precipitates were washed with 25 mL of ethanol for 6 times and dried at 333 K for 24 h prior to investigation.

The 4MZ sample was prepared by co-precipitation, according to the procedure described in a previous work [27].

2.3. Catalyst characterization

X-ray diffraction patterns were registered from the powdered samples by a Phillips X'Pert diffractometer, operating at Cu Kα line ($\lambda = 0.154$ nm) in the range of 2θ between 20 and 70°. Thermoanalytical investigation of the complex was carried out using simultaneous TG/DSC thermal analyzer Netzsch 449F1. The powdered sample was placed in the platinum crucible and heated in air from room temperature to 1273 K with a heating rate of 5 K/min. FTIR spectra were registered by a Bruker Tensor 27 spectrometer in the range of 400–4000 cm^{-1} from the pellets of the complex and mixed oxides powdered with KBr with a resolution of 4 cm^{-1}. The textural characterization was carried out by nitrogen physisorption at 77 K in the Micromeritics ASAP 2020 surface area and porosity analyzer. Before analysis, the samples were outgassed at vacuum conditions (<10^{-3} kPa) at 473 K for 4 h. Surface area was obtained from the BET method, whereas the pore size distribution and total pore volume were obtained from the BJH approach. The strength and distribution of the basic/acid sites were determined by temperature programmed desorption of preadsorbed CO_2 and NH_3, respectively, in a MicromeriticsTPD/TPR 2900 apparatus. Samples (10 mg) were pretreated in He at 723 K for 2.5 h and exposed to CO_2 or NH_3 (2.5% NH_3 in He) stream at 298 K temperature until saturation coverage was reached. Weakly adsorbed CO_2 or NH_3 was removed by flushing with He at the same temperature for about 1.3 h. The temperature was then increased at a linear rate of 5 K/min from 298 K to 723 K and the CO_2 or NH_3 desorption was monitored by mass spectrometry. An Oxford Instrument EDS attached to a Jeol 6460LV scanning electron microscope was used for determining the elemental composition of the oxides. The surface composition of the mixed oxides was measured by X-ray Photoelectron Spectroscopy (XPS), using a SPECS system equipped with a Hemispherical Phoibos detector operating in a constant pass energy, using Mg-Kα radiation ($h\cdot\upsilon = 1253.6$ eV).

2.4. Acetone self-condensation

A 150 mg sample of each catalyst was placed in a 0.4 cm i.d. U-shaped quartz tube located in a PID- controlled furnace. This reactor was connected to the reaction initial gas flow. The acetone was injected by a syringe pump as a liquid in a He flow (0.05 L/min) and vaporized in situ, obtaining a volume concentration of 3.2%. Outgoing gases from the reactor were analyzed online by a Shimadzu GC-2010 gas chromatograph with a FID detector. Before any batch, the catalyst was pretreated in He at 723 K for 1 h. The acetone gas

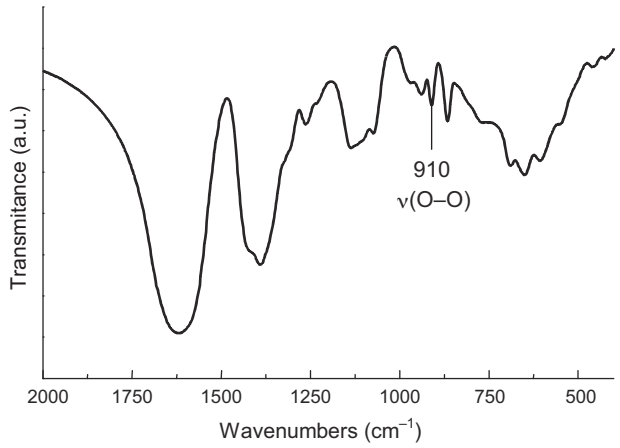

Fig. 1. FTIR spectra of the precursor of 1MZ sample.

phase condensation was studied in a temperature range from 473 to 723 K with steps of 50 K. More details about the reaction procedure, the reactor configuration and equipment were described in previous studies [32].

3. Results and discussion

3.1. Catalyst characterization

3.1.1. Investigation of the peroxocomplexes

Preliminary experiments established that dissolution of the precipitates occurs only for Mg/Zr ratios between 1 and 3. An increase in the magnesium content leads to the formation of the precipitate at the first stage of synthesis, which cannot be dissolved in the hydrogen peroxide solution. Contrary, lower amounts of magnesium in the starting solution cause the formation of complexes containing undesirable sodium ions in large excess.

The chemical composition of the prepared oxides was analyzed by EDS (Table 1), concluding that the Mg content is equal or slightly lower than predicted. A similar variation was already reported in the literature, being attributed to the elimination of highly dispersed $Mg(OH)_2$ species during the washing step [30]. A residual amount of sodium (<1 wt%) was also detected. Surface composition was analyzed by XPS and the results are also listed in Table 1. In all samples it is observed an enrichment of Mg on the surface. The precursor for 1MZ sample has been analyzed by FTIR and TG/DSC techniques, in order to show the formation of the peroxocomplex and reveal some features of its thermal decomposition. The FTIR spectrum of the prepared complex (Fig. 1) shows the main absorbance peaks corresponding to symmetric stretching of O=C–O at 1630 cm^{-1} and asymmetric ones at 1395 cm^{-1}, which are attributed to a citrate ligand, and also a characteristic band at 910 cm^{-1}. This last absorption can be attributed to the presence of peroxo-groups in the complex. In this way, in pure H_2O_2, O–O stretching vibration corresponds to a band at 877 cm^{-1}, but in complexes it might appear at lower or greater wavenumbers [33]. The data on the positions of O–O stretching vibrations in IR spectra of metal peroxocomplexes are not unequivocal. Tarafder et al. [34] observed O–O band vibrations at 840 cm^{-1}. Other researchers [35] assigned the band at 850 cm^{-1} to ν(O–O). In this way, the band at 860 cm^{-1} was reported to be a characteristic band of ν(O–O) in zirconium peroxocomplexes [36], which is similar to the results obtained for titanium peroxocitrate [37]. However, it is known that O–O bands can be observed at wavenumbers as high as 935 cm^{-1} [33]. Thus, we can suggest that the dissolution of the precipitate prepared from zirconium and magnesium salts in hydrogen peroxide leads to the formation of the zirconium peroxocomplex with magnesium in its cationic form, the stability of the complex being provided by the addition of citric acid. It is highly probable that the synthesized complexes have compositions and structures similar to those described previously for barium–titanium peroxocitrates [38].

Thermogravimetric analyses reveal that the isolated complex decomposes in two main steps. A typical profile (MZ1) is shown in the Supplementary Information, all the materials prepared by this procedure presenting similar profiles. The first one, occurring at temperatures before 473 K and having mass loss of approximately 15%, corresponds to dehydration and removal of the excess of the ligand. The second stage of decomposition in the range of 673–773 K is accompanied by an exothermic effect on the DSC curve; ascribed to the oxidation of the organic part of the complex. Furthermore, a maximum at 503 K is observed which could be attributed to the rupture of the O–O bridges and transition of the singlet oxygen to O^{2-} state, in agreement with the results obtained by Ichinose et al. [39], in their studies about peroxotitanates. A third broad exothermic peak is also observed in the range of 928–1028 K, attributed to the polymorphic transitions in zirconia and magnesia systems (Supplementary Information).

3.1.2. XRD and FTIR studies of MgO/ZrO_2

X-ray diffraction analysis of the prepared samples detects the presence of poorly crystalline phases, which can be attributed to: cubic MgO phase (ICDD PDF2 99-200-4113), cubic or tetragonal zirconia (ICDD PDF2 99-101-0922, ICDD PDF2 00-042-1167) undistinguishable due to broad and inseparable peaks, or the magnesia-stabilized zirconia phase with a general formula $Mg_xZr_{1-x}O_{2-x}$ (ICDD PDF2 00-080-0967 and 00-080-0964) (Fig. 2a). In the 1MZXRD pattern, the presence of cubic magnesia is hardly noticeable, but at higher Mg/Zr ratios the separation of crystalline MgO from the mixed oxide becomes more obvious. The crystallite size of magnesia reaches 7 nm in the 3MZ mixed oxide. The (1 1 1) reflection of cubic/tetragonal zirconia phase is shifted to higher 2θ degrees on the XRD of all magnesia–zirconia samples in comparison with pure zirconia prepared via similar procedure (Fig. 2a), that indicates the formation of cubic magnesia-stabilized zirconia phase. The crystallite size of $Mg_xZr_{1-x}O_{2-x}$, estimated by Scherrer equation is found to be in the range of 3–4 nm for all MgO/ZrO_2 ratios. This shifting (Fig. 2b), caused by incorporation of magnesium ions in crystalline lattice of zirconia, was already noticed. Contrary to this case, Sádaba et. al [30] found this peak continuously shifted to the higher 2θ degrees with the increasing MgO/ZrO_2 ratios up to 4.88, indicating higher degree of incorporation of magnesium ions into the zirconia matrix. However, the ability of zirconia matrix to accommodate magnesium ions is limited, as the highest Mg/Zr ratio crystalline $Mg_xZr_{1-x}O_{2-x}$ possesses, according to ICDD PDF2 database, is 0.4/1. The presence of $Mg_xZr_{1-x}O_{2-x}$ phase was not detected in 4MZ prepared by co-precipitation and only peaks corresponding to periclase MgO and tetragonal ZrO_2 were identified [27]. The difference in the formation of the $Mg_xZr_{1-x}O_{2-x}$ phase in the materials prepared via co-precipitation and peroxo-method can be explained in the following way. During the co-precipitation, the incorporation of magnesium into amorphous zirconia could be accompanied by the formation of magnesium hydroxide. The increase of magnesium ions concentration promotes their inclusion in ZrO_2 lattice to the higher extent, when the other part of magnesium ions is precipitated in the form of hydroxide. The process of structure formation of oxide phase from the peroxocomplex is different. In this case, zirconia peroxo-species and magnesium ions are parts of the same structural unit; this feature ensures high molecular homogeneity of the material, as the oxide phase forms directly by complex decomposition, avoiding the stage of precipitation of metal hydroxides. This justifies the highest incorporation of magnesium ions into ZrO_2 lattice of the 1MZ sample.

Table 1
Morphological properties of magnesia–zirconia samples.

Samples	Chemical composition	Mg/Zr surface atomic ratio (XPS)	Surface area, S_{BET}, m^2/g	Pore volume V_p, cm^3/g	Mean pore diameter D_p, Å	Crystallite sizes of $Mg_xZr_{1-x}O_{2-x}$; MgO, nm
1MZ	$Mg_1Zr_1Na_{0.05}$	1.18	87	0.08	31	3; –
2MZ	$Mg_{1.8}Zr_1Na_{0.01}$	4.30	48	0.08	136	3; –
3MZ	$Mg_{2.6}Zr_1Na_{0.1}$	5.08	30	0.07	102	3; 7
4MZ[a]	$Mg_{4.5}Zr_1Na_{0.02}$	11.7	78	0.8	342	–; 11

[a]Data taken from the study [27] for the bulk magnesia–zirconia prepared via precipitation method. Chemical composition was obtained by EDS for the peroxocomplexes. For sample 4MZ, by ICP-OES.

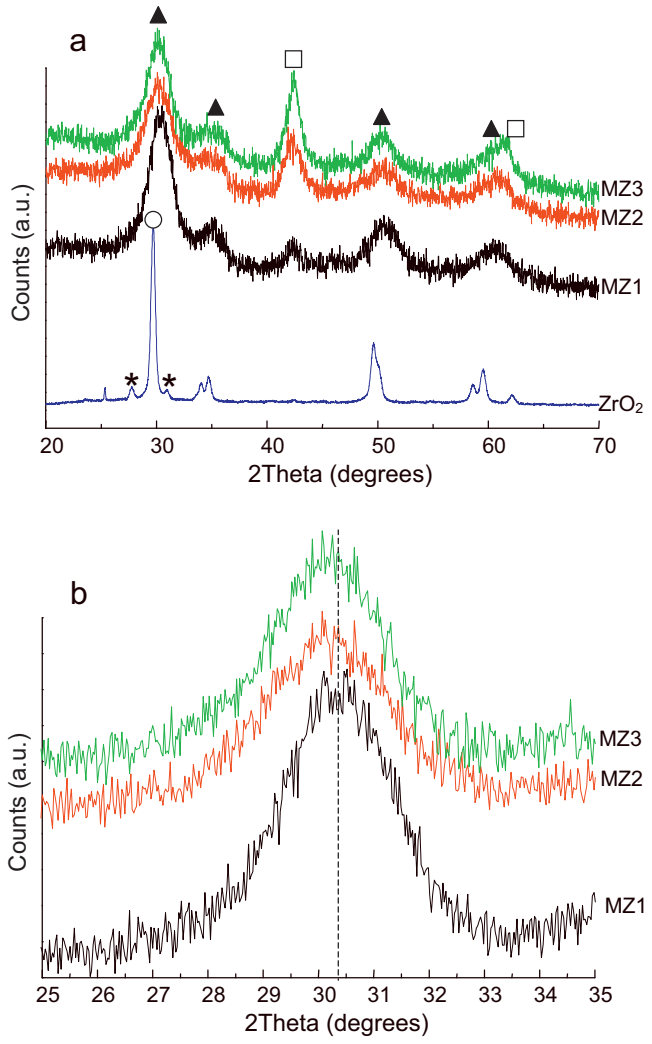

Fig. 2. XRD patterns of the zirconia–magnesia samples (a), and enlarged region of 2θ values showing the reflection attributed to $Mg_xZr_{1-x}O_{2-x}$ cubic phase (b). Symbols: cubic MgO (□);tetragonal zirconia (○);monoclinic zirconia (*);cubic $Mg_xZr_{1-x}O_{2-x}$(▲).

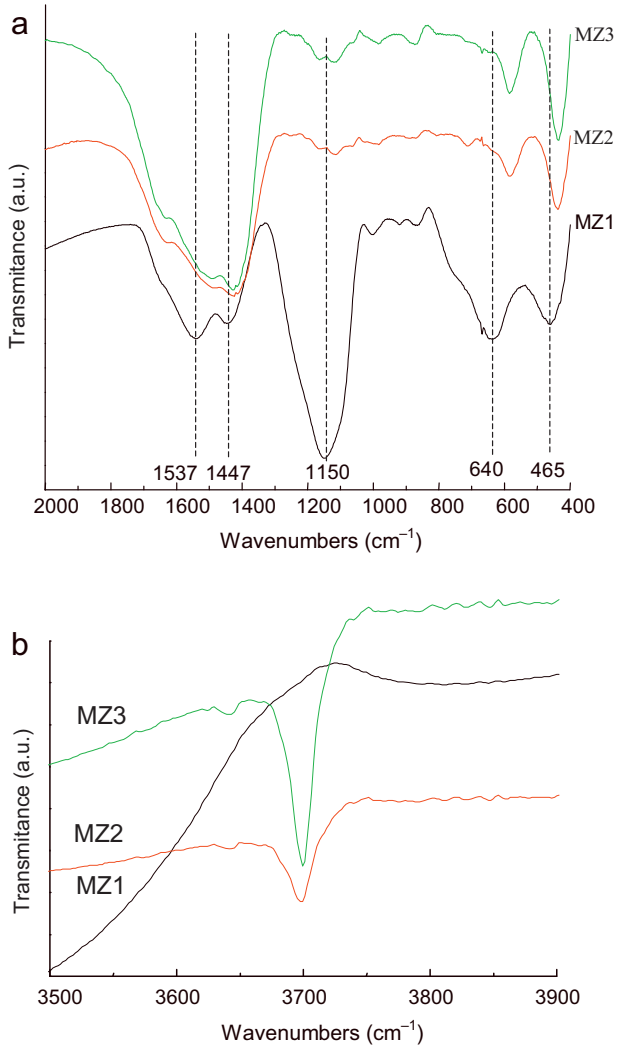

Fig. 3. FTIR spectra of the magnesia–zirconia samples (a) and the region of OH-groups stretching vibrations (b).

The most broad and intense doubling peak in the IR spectra of all samples (Fig. 3a) is observed in the range of 1600–1400 cm^{-1} corresponding to Mg–O stretching and bidentate carbonate bonded to the surface of oxides. Absorption at 1150 cm^{-1}, present in all spectra, can be attributed to CO_3^{2-} stretching, and it is found to have the highest intensity in the spectrum of 1MZ sample. Probably, due to the adsorption of carbonate species on the strong basic Mg–O–Zr centers of the $Mg_xZr_{x-1}O_{2-x}$ mixed oxide phase. The bands at 550–630 and 430–450 cm^{-1} can be attributed to the Mg–O vibrations in the crystalline periclase. It is worth mentioning that the band near 3700 cm^{-1} (Fig. 3b) does not appear for 1MZ sample. The absorption at this range of wave numbers unambiguously corresponds to the vibration of OH groups bonded to magnesium atoms. It is more likely that Mg–OH groups have been formed in the result of re-hydroxylation of MgO surface with atmospheric water vapors. The success in the incorporation of magnesium atoms in the zirconia lattice via bridged oxygen bonded to zirconium, can satisfactorily explain the absence of this band in the 1MZ spectrum. This observation also supports the formation of more homogeneous mixed magnesia–zirconia phase in these samples, made on the basis of XRD analysis.

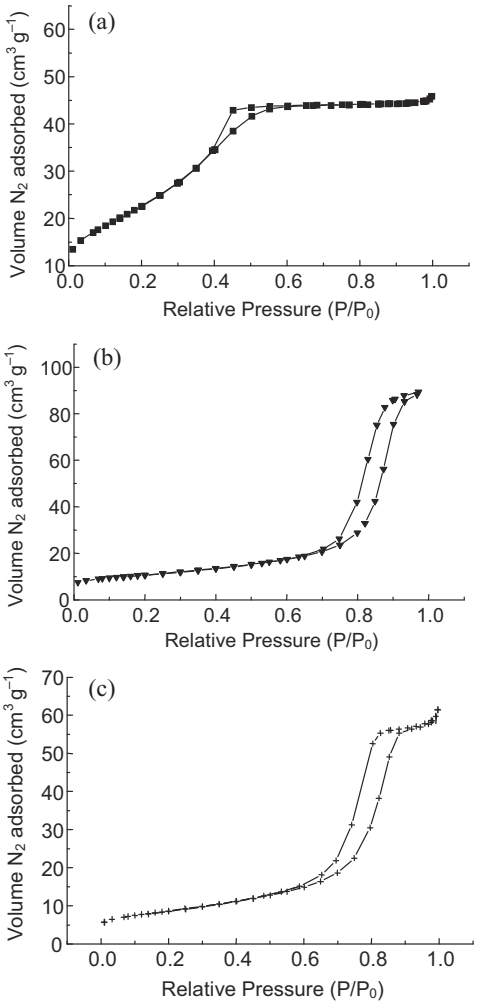

Fig. 4. Adsorption–desorption isotherms of the magnesia–zirconia samples: (a) 1MZ, (b) 2MZ and (c) 3MZ.

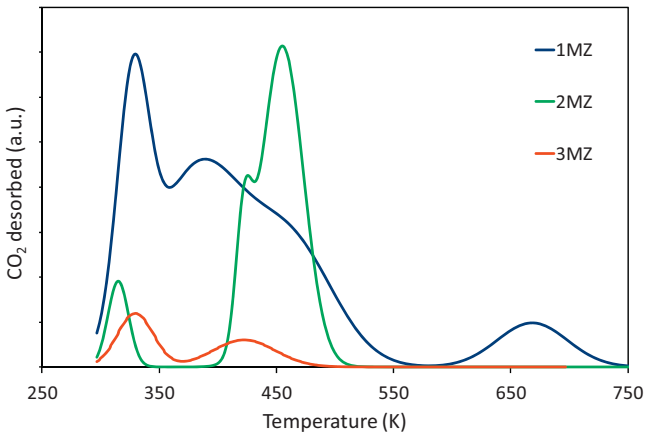

Fig. 5. CO_2-TPD curves of the magnesia–zirconia samples.

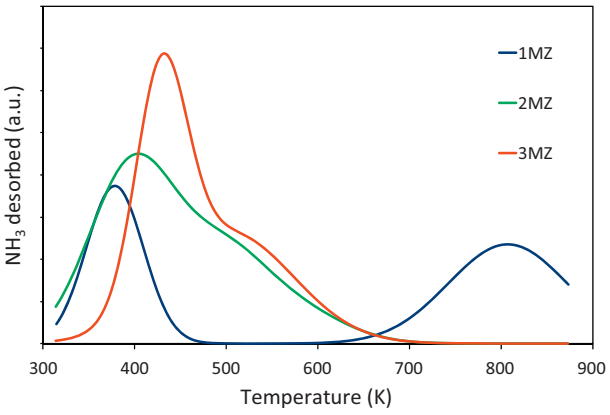

Fig. 6. NH_3-TPD curves of the magnesia–zirconia samples.

3.1.3. *Textural and morphological properties*

Textural properties of the samples are summarized in Table 1. Nitrogen adsorption–desorption isotherms determined at 77 K (Fig. 4) correspond in all the cases to type IV (mesoporous solids), according to IUPAC classification. The hysteresis loops are rather narrow and vertically oriented in the case of 2MZ and 3MZ, being associated to type H1 – porous materials exhibiting a narrow distribution of relatively uniform (cylindrical pores). Same type of loop was previously observed in 4MZ prepared by co-precipitation. In the case of 1MZ, the hysteresis loop shows the typical shape of H_2 type, typical of more complex pore networks consisting of pores with ill-defined shape and wide pore size distribution. Comparing the samples obtained by the peroxocomplex route with the bulk magnesia–zirconia prepared via precipitation method, a slight increase in surface area and pore volume is observed for the 1MZ sample—the sample with the highest incorporation of magnesium ions into ZrO_2 lattice sample, according to XRD patterns—, whereas higher magnesium content decreases the specific surface area. Contrary, Sádaba et al. [30] noticed that the surface area increased with magnesium content. The surface area is related to the fraction of crystalline MgO phase. In that work, the crystallization of periclase goes through the formation of the intermediate highly dispersed magnesium hydroxide, whose further dehydration resulted in the MgO phase [30]. This method could allow the formation of porous magnesia with more developed surface in comparison to the method proposed in the present study, where MgO is formed avoiding hydrolysis and precipitation stage.

3.1.4. *Basic and acid properties*

CO_2-TPD profiles of the magnesia–zirconia oxides are depicted in Fig. 5, whereas the concentrations and strength-distributions of the basic sites are summarized in Table 2. Comparing all the results with the basicity distribution of the bulk 4MZ prepared by co-precipitation method [27], a noticeable decrease in both, concentration and strength, can be observed. Materials prepared by the peroxo-route present mainly weak and medium-strength basic sites (bicarbonates and bidentates) and the concentration of these sites decreases as Mg/Zr ratio increases: from 66 μmol/g (1MZ) to 25 μmol/g (3MZ). There is not an important difference in the desorption temperatures among the three materials. These results are in agreement with FTIR experiments. The medium strength basic sites are the main, corresponding to the most intense peak (1600–1400 cm^{-1}) attributed to bidentate carbonates bonded to the oxide surface. These bidentate carbonates require the participation of an adjacent cationic site (M^+–O^{2-} pairs, medium strength base sites), that is, the presence of an associated acid site, as demonstrated using microcalorimetric studied with hydrotalcite-derived Mg–Al mixed oxides [40]. Likewise, 1MZ sample exhibits also the strongest basic sites, in agreement with the band at 1150 cm^{-1} observed for this material.

The analysis of the acidity was carried out by NH_3-TPD. Profiles obtained are shown in Fig. 6 whereas the distribution of acid sites was summarized in Table 2. The material prepared by co-precipitation (4MZ) showed higher acidity than the peroxocomplex route prepared materials [27]. Likewise, the acidity of the 4MZ

Table 2
Basic and acid properties of magnesia–zirconia samples.

Samples	Basic sites, CO_2-TPD, μmol/g (K)			Acid sites, NH_3-TPD, μmol/g (K)		
	Bicarbonate	Bidentate	Monodentate	Weak (<503)	Medium (503 < T < 673)	Strong (>673)
1MZ	21 (330)	45 (458)	6 (666)	34 (378)	–	45 (808)
2MZ	11 (317)	34 (455)	–	59 (399)	38 (505,569)	–
3MZ	12 (329)	13 (423)	–	49 (428)	61 (574)	–
4MZ[a]	–	121 (444)	13 (585)	62 (353)	74 (566)	–

[a]Data taken from the study [27] for the bulk magnesia–zirconia prepared via precipitation method.

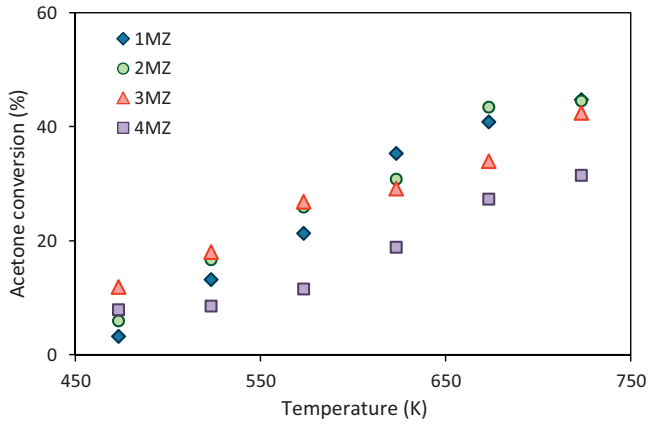

Fig. 7. Activity for the acetone condensation over the different Mg–Zr catalysts.

sample showed similar trends, with different concentrations but similar strength distributions, to 2MZ and 3MZ samples. In all cases, the acidic sites are distributed into weak and medium strength acid sites. In the case of 1MZ catalyst, medium-strength acid sites disappeared and a desorption peak a temperatures above 800 K appeared. From a previous work [27], it was concluded that strong acid sites do not participate in the reaction, thus this peak will be not considered.

3.2. Reaction studies

The acetone gas-phase condensation was carried out at temperatures between 373 and 723 K using the different Mg/Zr materials as catalysts. The different compounds identified were congruent with the general mechanism proposed for this reaction. This mechanism is summarized in Scheme 1. The condensation reaction of acetone forms diacetone alcohol. A subsequent dehydration of this compound leads to either isomesityl oxide or mesityl oxide. Condensation of these C6 compounds with acetone forms phorones (C9), which rearrange to yield cyclic C9 compounds called isophorones. It was previously studied how the distribution of acid and basic sites in the catalyst condition the selectivity of each product obtained in this reaction [28]. The absence of diffusional limitations at working conditions was corroborated using the Thiele modulus modified by Weisz [41] and the negligible acetone conversion at these conditions without any catalysts was previously confirmed [28]. It should be also noted that the density of the studied materials is very similar, leading to similar catalytic bed lengths, and discarding any variation of the effective residence time when using different catalysts.

The evolution of the acetone conversion with the temperature using the different catalysts is plotted in Fig. 7. Results obtained with 4MZ were also plotted to easily discuss the differences between both preparation methods. The acetone conversion increases with the temperature, reaching values for the peroxo-method prepared MgZr oxides higher in all cases than for the bulk co-precipitated MgZr oxide. The conversion at 723 K reaches the 44% for 1MZ, 2MZ and 3MZ, whereas the bulk oxide did not exceed 35%. Selectivity to the main reaction products–diacetone alcohol (C6), mesityl oxide (C6), phorones (C9), isophorones (C9) and mesitylene (C9) are summarized in Table 3 for two temperatures, as well as the carbon balance.

Selectivities below 573 K were mainly towards C6 products, whereas at 723 K, the C9 compounds become more important. Selectivity towards trimers at the highest temperature, reaches the value of 30.1, 20.2 and 4.9% towards phorones (P), mesitylene (M) and isophorones (IP), respectively. For comparative purposes, the amount of IP obtained is lower than over Mg-Al oxides (13.9%) [42] and Mg–Zr oxides (18%) [28]. Further, it is interesting to point out that the selectivities towards C9 compounds are slightly higher (55.2 for 1MZ versus 42% for Mg–Zr supported on high surface area graphite), although the conversion is lower (44.8 versus 54%) [28]. The values here obtained of C9 compounds are similar to that obtained over a high surface area MgO (53.8%), obtained by an hydrothermal treatment [32].

Focusing on the peroxo-method prepared MgZr oxides, it is observed that the conversion reached, especially at the highest temperature, is very similar in the three cases, being more notorious the differences in selectivities. At temperatures lower than 523 K, only C6 products are formed in relevant concentrations. Only the 1MZ catalyst, the material with the lowest conversion at this temperature, reaches a 17.6% of selectivity towards phorones. In all cases, the diacetone alcohol follows the typical profile of a primary product, whose selectivity reaches a maximum and decreases by the decomposition into other products. Among MO and IMO, mesityl oxide is the main product at these conditions, following IMO an unclear trend. The formation of DAA is catalyzed by medium strength basic sites, and its decomposition into MO or IMO needs acid-basic pairs. These vicinal M^+–O^{2-} sites are formed by the oxygen anion, a medium-strength base, and the M+, weakly acid. Likewise, it was shown in previous works that add to medium, the presence of weak basic sites enhances this reaction [28]. 1MZ sample exhibits the highest amount of bidentate and also bicarbonate centers, thus the highest reaction extension. Comparing the results of the Mg–Zr oxides prepared by the peroxo-method with those previously published on coprecipitated Mg–Zr oxides, it is evident that the materials presented in this work have a more homogeneous distribution of basic and acid sites, in agreement with XRD analysis, where a more homogeneous mixed magnesia–zirconia phase in these samples was observed.

At 723 K, the selectivity towards C6 decreases and C9 compounds become more important, reaching for 1MZ selectivities to C9 of 55.2%. The first trimer formed is the phorone, which reacts to form either isophorones or mesitylene. Isophorones, the most valuable product, are obtained in lower extension than over co-precipitated Mg–Zr oxides of Mg–Al oxides. This step requires the presence of strong basic sites, only presented on 1MZ catalyst, surprisingly, with the lowest selectivity towards these compounds. However, it is notorious the high selectivity towards mesitylene, product that can be obtained by two different routes. It can be formed from linear phorones, involving basic and acid sites [28], but also from isophorones, involving only acid sites. Thus, the high

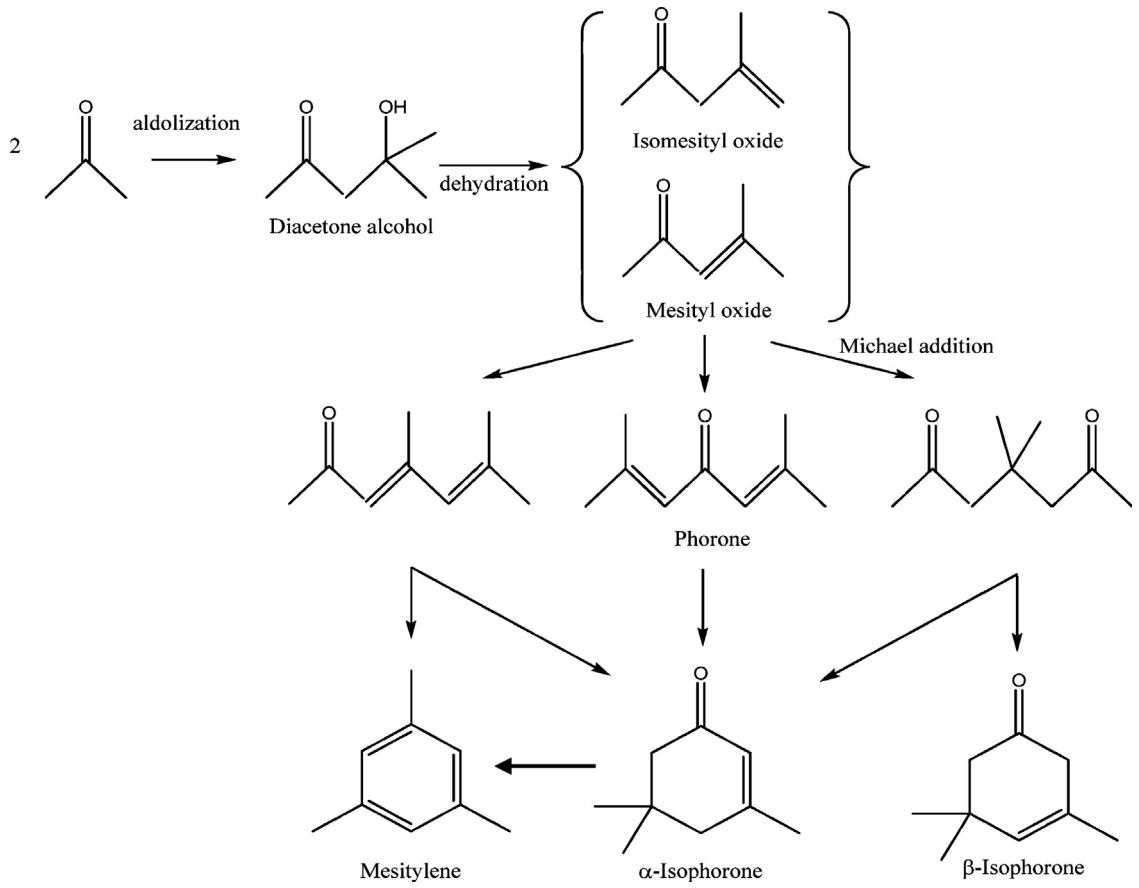

Scheme 1. Reaction mechanism for the acetone self-condensation.

Table 3
Evolution of selectivity of acetone condensation towards the reactions products at three temperatures: diacetone alcohol (DAA), isomesityl oxide (IMO), mesityl oxide (MO), phorone (P), mesitylene (M) and isophorone (IP).

Catalyst	Conversion (%)/carbon balance (%)		Selectivity (%)											
			DAA		IMO		MO		P		M		IP	
	523 K	723 K	523 K	723 K	523 K	723 K	523 K	723 K	523 K	723 K	523 K	723 K	523 K	723 K
1 MZ	13.3/95.0	44.8/91.5	11.1	7.6	3.9	1.0	64.2	36.3	17.6	30.1	3.2	20.2	0.0	4.9
2 MZ	16.7/96.0	44.6/82.2	13.3	7.7	0.0	0.1	79.4	71.3	4.5	3.9	2.1	9.8	0.8	7.3
3 MZ	18.1/85.8	42.5/80.5	13.1	24.8	0	0.1	82.1	53.6	4.7	6.8	0.0	6.2	0.0	8.6
4 MZ[a]	14.5/94.6	31.5/91.3	1.3	8.0	2.1	0.5	76.7	69.6	1.6	0.5	2.2	0.1	16.1	25.5

[a]Data taken from the study [28] for the bulk magnesia–zirconia prepared via precipitation method and used as the catalyst for acetone self-condensation.

selectivity here observed towards mesitylene at 723 K is in good agreement with the isophorones selectivity profile and with the relevant concentration of strong acid sites observed in 1MZ sample. By contrasts, on 2MZ and 3MZ, mesitylene could be formed mainly from phorones, route which requires the presence of basic and weak acid sites, present in these materials (Table 2)

Comparing the results obtained with these materials and with the bulk oxide (4MZ), it should be noted that although the conversions are only slightly lower with the 4MZ material, selectivity patterns are completely different. In general terms, 4MZ shows higher selectivity towards isophorones, and lower to the formation of phorones and mesitylene. In the most accepted mechanisms for acetone condensation, it is assumed that intramolecular aldol condensations (needed for the formation of isophorones) require higher strength of basic sites than the acetone aldol condensation for MO and IMO formation [28]. Obtained results suggest that the strength of the basic sites in the materials prepared by the peroxo-mediated procedure is enough for aldol condensation, but not enough for the intramolecular condensation. From the point of view of the acid sites distribution, both kinds of MgZr oxides present a very similar acidity pattern. However, the ratio between the amount of acid and basic sites is higher for the mixed oxides prepared by the peroxo-mediated procedure. In good agreement with this fact, mesitylene selectivity increases for these materials. It should be noted that mesitylene formation from phorone needs the presence of acid sites [28].

4. Conclusions

We propose in this work a new peroxo-mediated procedure for the preparation of mixed magnesia–zirconia catalysts. The dissolution of the magnesia-zirconia hydrogel in hydrogen peroxide in presence of citric acid leads to the formation of the amorphous peroxocomplex, whose stability and solubility are ensured by the addition of carboxylic acid. This method provides a high degree of incorporation of magnesium ions into the crystalline

lattice of zirconia, thus forming cubic magnesia-stabilized zirconia phase with a general formula$Mg_xZr_{x-1}O_{2-x}$. With the increasing of magnesia content in the samples the separation of the periclase from the mixed oxide phase becomes more noticeable, whereas no significant changes in the $Mg_xZr_{x-1}O_{2-x}$lattice parameters can be observed. The decrease of surface area in the samples with Mg/Zr molar ratio higher than 1 is attributed to higher crystallinity of magnesium oxide. Total basicity and acidity of the prepared materials are found to be lower than it is for precipitated mixed oxide. Only the 1MZ sample exhibits strong basic and acid sites. The acetone gas-phase self condensation results evidence the homogeneous distribution of acid and basic sites on the Mg–Zr oxides prepared by the peroxo-complex route. Likewise, it was observed that the selectivity towards mesitylene is especially important for the 1MZ sample, catalyst with the highest amount of both medium and high strength basic sites and also strong acid sites.

Acknowledgement

This work was supported by the Spanish Government (contract CTQ2011-29272-C04-02).

Appendix A. Supplementary data

Supplementary material related to this article can be found, in the online version, at http://dx.doi.org/10.1016/j.apcata.2014.03.008.

References

[1] S. Yoon, T. Noh, W. Kim, J. Choi, H. Lee, Ceram. Int. 39 (2013) 9247–9251.
[2] L. Hao, J. Lawrence, Mater. Sci. Eng. A364 (2004) 171–181.
[3] X. Jiao, L. Li, N. Zhao, F. Xiao, W. Wei, Energ. Fuels 27 (2013) 5407–5415.
[4] G. Parameswaram, M. Srinivas, B. HariBabu, P.S. Sai Prasada, N. Lingaiah, Catal. Sci. Technol. (2013), http://dx.doi.org/10.1039/C3CY00532A.
[5] V. Eta, P. Mäki-Arvela, J. Wärnå, T. Salmi, J.-P. Mikkola, D.Y. Murzin, Appl. Catal. A 404 (2011) 39–46.
[6] M.B. Gawande, A.K. Rathi, P.S. Branco, T.M. Potewar, A. Velhinho, I.D. Nogueira, A. Tolstogouzov, C.A.A. Ghummane, O.M.N.D. Teodoro, RSC Adv. 3 (2013) 3611–3617.
[7] C.J. Barrett, J.N. Chheda, G.W. Huber 1, J.A. Dumesic, Appl. Catal. B 66 (2006) 111–118.
[8] S. Liu, X. Zhang, J. Li, N. Zhao, W. Wei, Y. Sun, Catal. Commun. 9 (2008) 1527–1532.
[9] D. Jiang, G. Pan, B. Zhao, G. Ran, Y. Xie, E. Min, Appl. Catal. A 201 (2000) 169–176.
[10] V.V. Ordomsky, V.L. Sushkevich, I.I. Ivanova, J. Mol. Catal. A 333 (2010) 85–93.
[11] M.A. Aramendia, V. Boráu, C. Jiménez, A. Marinas, J.M. Marinas, J.A. Navio, J.R. Ruiz, F.J. Urbano, Colloid. Surf. A 234 (2004) 17–25.
[12] M.B. Gawande, P.S. Branco, K. Parghi, J.J. Shrikhande, R.K. Pandey, C.A.A. Ghumman, N. Bundaleski, O.M.N.D. Teodorod, R.V. Jayaramb, Catal. Sci. Technol. 1 (2011) 1653–1664.
[13] H. Gocmeza, H. Fujimori, Mater. Sci. Eng. B 148 (2008) 226–229.
[14] T. Settu, Ceram. Int. 26 (2000) 517–521.
[15] M.A. Aramendia, V. Borau, C. Jiménez, A. Marinas, J.M. Marinas, J.R. Ruiz, F.J. Urbano, J. Mol. Catal. A 218 (2004) 81–90.
[16] R.H.R. Castro, P.J.B. Marcos, A. Lorriaux, M.C. Steil, L. Gengembre, P. Roussel, D. Gouvea, Chem. Mater. 20 (2008) 3505–3511.
[17] M. Tahmasebpour, A.A. Babaluo, M.K.R. Aghjeh, J. Eur. Ceram. Soc. 28 (2008) 773–778.
[18] I.V. Krivtsov, M.V. Ilkaeva, V.V. Avdin, D.A. Zherebtsov, J. Non Cryst. Solids 362 (2013) 95–100.
[19] I. Sádaba, M. Ojeda, R. Mariscal, R. Richards, M. Lopez Granados, Chem. Phys. Chem. 13 (2012) 3282–3292.
[20] Lisa. C. Klein (Ed.), Sol–Gel Optics: Processing and Applications, Kluwer Academic Publisher, 1994.
[21] M. Kakihana, M. Kobayashi, K. Tomita, V. Petrykin, Bull. Chem. Soc. Jpn. 83 (2010) 1285–1308.
[22] J.-Y. Piquemal, E. Briot, J.-M. Brégeaultc, Dalton Trans. 42 (2013) 29–45.
[23] Y. Gao, Y. Masuda, H. Ohta, K. Koumoto, Chem. Mater. 16 (2004) 2615–2622.
[24] J.H. Park, Y.B. Yoo, K.H. Lee, W.S. Jang, J.Y. Oh, S.S. Chae, H.K. Baik, ACS Appl. Mater. Interfaces 5 (2013) 410–417.
[25] L. van Rij, L. Winnubst, L. Jun, J. Schoonman, J. Mater. Chem. 10 (2000) 2515–2521.
[26] M.D. Gonçalves, R. Muccillon, Ceram. Int. 40 (2014) 911–917.
[27] L. Faba, E. Díaz, S. Ordóñez, Appl. Catal. B 113-114 (2012) 201–211.
[28] L. Faba, E. Díaz, S. Ordóñez, Appl. Catal. B 142–143 (2013) 387–395.
[29] P.J. Darda, V.V. Ranade, Chem. Eng. J. 207–208 (2012) 349–367.
[30] I. Sádaba, M. Ojeda, R. Mariscal, J.L.G. Fierro, M. Lopez Granados, Appl. Catal. B101 (2011) 638–648.
[31] I.V. Krivtsov, M.V. Ilkaeva, V.D. Samokhina, V.V. Avdin, S.A. Khainakov, D.A. Uchaev, J.R. Garcia, J. Sol–Gel Sci. 63 (2013) 665–669.
[32] M. León, L. Faba, E. Díaz, S. Bennici, A. Vega, S. Ordóñez, A. Auroux, Appl. Catal. B 147 (2014) 796–804.
[33] J. Muhlebach, K. Muller, G. Shwarzenbach, Inorg. Chem. 9 (1970) 2381–2390.
[34] M.T.H. Tarafder, P. Bhattacharjee, A.K. Sarkar, Polyhedron 1 (1992) 795–798.
[35] D.D. Agarwal, R. Jain, R.P. Bhatnagar, S. Srivastava, Polyhedron 9 (1990) 1405–1409.
[36] A.C. Dengel, W.P. Griffith, Polyhedron 8 (1989) 1371–1377.
[37] I. Truijen, A. Hardy, M.K. Van Bael, H. Van den Rul, J. Mullens, Thermochim. Acta 456 (2007) 38–47.
[38] M. Tada, K. Tomita, V. Petrykin, M. Kakihana, Solid State Ionics 151 (2002) 293–297.
[39] H. Ichinose, M. Terasaki, H. Katsuki, J. Ceram. Soc. Jpn. 107 (1996) 715–718.
[40] M. León, E. Díaz, S. Bennici, A. Vega, S. Ordóñez, A. Auroux, Ing. Eng. Chem. Res. 49 (2010), 3663–3671.
[41] P.B. Weisz, Science 179 (1973) 433.
[42] S. Ordóñez, E. Díaz, M. León, L. Faba, Catal. Today 167 (2011) 71–76.